Full-Brain T_1 Mapping through Inversion Recovery Fast Spin Echo Imaging with Time-Efficient Slice Ordering

David C. Zhu[1]* and Richard D. Penn[2]

Brain T_1 mapping has important clinical applications in detecting brain disorders. Conventional T_1 mapping techniques are usually based on inversion recovery spin echo (IRSE) imaging or its more time-efficient counterpart inversion recovery fast spin echo (IRFSE) imaging because they can deliver good image quality. Multiple inversion times are required to accurately estimate T_1 over a wide range of values. Without acquisition optimization, both the IRSE and the IRFSE T_1 mapping techniques require long scan times to image the whole brain. To reduce the scan time and maintain the quality of the T_1 maps, we propose a new full-brain T_1 mapping pulse sequence based on a multislice inversion recovery fast spin echo imaging using a time-efficient slice ordering technique. Magn Reson Med 54: 725–731, 2005. © 2005 Wiley-Liss, Inc.

Key words: T_1 mapping; IRFSE; spin echo; brain; time efficient slice ordering

Brain T_1 mapping is important in detecting brain pathology. Conventional T_1 mapping techniques are usually based on inversion recovery spin echo (IRSE) imaging or its more time-efficient counterpart inversion recovery fast spin echo (IRFSE) imaging because they can deliver good image quality. Multiple inversion times are required to accurately estimate T_1 over a wide range of values. Without acquisition optimization, both the IRSE and the IRFSE T_1 mapping techniques require long scan times to image the whole brain. The new technique introduced here is to optimize the acquisition. It combines the time-efficient slice ordering (TESO) method similar to that proposed by Clare and Jezzard (1) and the good image quality of IRFSE (2). This combination should make high-quality full-brain T_1 mapping possible in a busy clinical environment. This development is valuable for clinical diagnosis and for the quantitative assessments of brain water under pathologic conditions like cerebral edema, hydrocephalus, and stroke (3–5). Our new T_1 mapping technique (TESO-IRFSE) has been evaluated with phantom and human studies on 3- and 1.5-T MRI systems.

METHODS

Pulse Sequence Design

IRFSE T_1 mapping, like other T_1 mapping techniques, requires multiple inversion times (TI) to accurately estimate T_1 over a wide range of values (1,3,4,6–9). Its conventional implementation follows a process of spin inversion, "waiting" for a TI time, and then data acquisition. The waiting time is the major cause of the long scan time for full-brain T_1 mapping. The TESO method is designed to minimize the waiting time but maintain the wide-range of TI choices suitable for accurate T_1 calculation.

The TESO-IRFSE technique is demonstrated in Fig. 1. Six TI steps (six TI choices for T_1 map generation) are used to generate T_1 maps at 12 slice locations. Six TI steps require six slice-ordering schemes. For each slice-ordering scheme, each train of slice acquisition starts with a nonselective Silver–Hoult adiabatic inversion RF pulse that provides a uniform inversion of spins even in the presence of a nonuniform B_1 field (10) and inverts spins within the entire sensitive volume of the head transmit coil. The use of nonselective inversion removes the slice profile mismatch problem that is common in T_1 calculation (8). After a fixed time delay (the first TI choice for some slices), acquisition starts with a multislice fast spin echo (FSE) pulse sequence. The 90° excitation and 180° refocusing RF pulses are time-truncated sinc pulses. After all phase encoding steps are completed with the first slice-ordering scheme, data are acquired with the second slice-ordering scheme. Data acquisition continues in the same fashion with the other four slice-ordering schemes. The TI increment is equal to the time between every other two slice acquisition lengths, each of which equals the time of repetition (TR) divided by the total number of slices. At each slice location, six images at different TI choices are acquired. For a general protocol design, the TESO-IRFSE technique requires that the total number of slices be equal to the multiplication of the number of TI steps by the number of slices in each TI increment.

Multiple echoes are acquired after each spin excitation in FSE imaging. Due to T_2 decay, image blurring is a common issue. It becomes more pronounced with the increase of echo train time and translates into an imprecise T_1 calculation. To reduce image blurring, a minimum TE (time of echo), which is equal to the echo spacing (ESP), is always selected in the TESO-IRFSE technique to achieve a symmetric k space acquisition. This selection also allows the center of k space to be located at the beginning of the echo train and thus maximizes the signal intensity and equivalently the signal-to-noise ratio (SNR). A simpler method to reduce FSE image blurring is to reduce the overall echo train time (ETL · ESP) by choosing a shorter echo train length (ETL) and/or a shorter ESP through a higher receiver bandwidth (11). A shorter ETL, however, reduces the scan time efficiency and a higher receiver bandwidth leads to lower SNR. The choice of an ETL of 4 with a receiver bandwidth of ±31.25 kHz appears to be a

[1]Department of Radiology, University of Chicago, Chicago, Illinois, USA.
[2]Department of Neurosurgery, University of Chicago, Chicago, Illinois, USA.
Grant sponsor: Brain Research Foundation at the University of Chicago; Grant sponsor: Medtronic, Inc.
*Correspondence to: David C. Zhu, Department of Radiology, MC 2026, University of Chicago, 5841 S. Maryland Avenue, Chicago, IL 60637, USA. E-mail: davidzhu@uchicago.edu
Received 21 July 2004; revised 6 April 2005; accepted 6 April 2005.
DOI 10.1002/mrm.20602
Published online 5 August 2005 in Wiley InterScience (www.interscience.wiley.com).

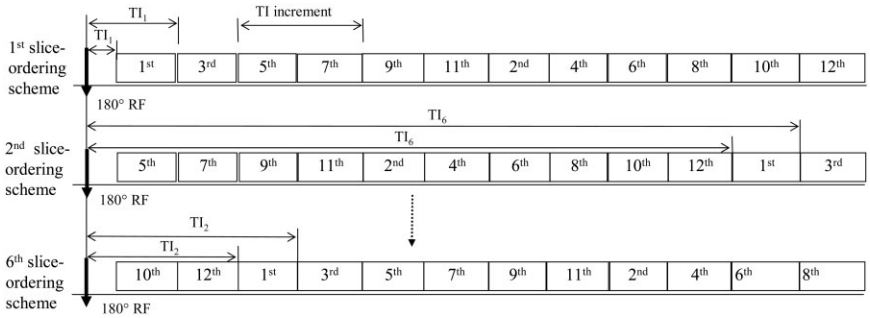

FIG. 1. Three of the six TI steps (TI_1, TI_2, TI_3, TI_4, TI_5, and TI_6) for the first and third slices are illustrated. Six slice-ordering schemes, with three of them shown, are needed to complete the six TI steps.

reasonable compromise. The choice of a proper ETL has also been discussed by Deoni et al. for T_1 mapping (9).

The existing multislice FSE echo train (12) is modified to replace the single gradient spoiler by a dual gradient spoiler at the end of each echo train (Fig. 2). Specifically, the first gradient spoiler is applied to dephase the net transverse magnetization. Then a 90° RF pulse is applied to nutate the recovered longitudinal magnetization back to the transverse plane. A gradient spoiler is applied again to dephase the transverse magnetization. The purpose of the dual spoiler is to have the longitudinal magnetization recovery restarting at zero; modeling the longitudinal magnetization evolution becomes simpler after reducing the dependency on the nature of the echo train, such as the unknown effective RF flip angles. The effective flip angles often deviate from the intended angles due to slice profile imperfection and tissue dielectric effects (13).

T_1 Calculation

The T_1 at a voxel or region of interest (ROI) is calculated based on the longitudinal magnetization recovery curve. Assuming the dual gradient spoiler performs as expected, the longitudinal magnetization right before the application of the nonselective inversion RF pulse is

$$M_{\text{Before\_IR}} = M_0(1 - e^{-T_{\text{SP\_to\ before\ IR}/T_1}}),$$

where M_0 = the longitudinal magnetization under fully relaxed conditions, and $T_{\text{SP\_to\_Before\_IR}}$ = the time between the end of the dual gradient spoiler and the application of the nonselective RF pulse.

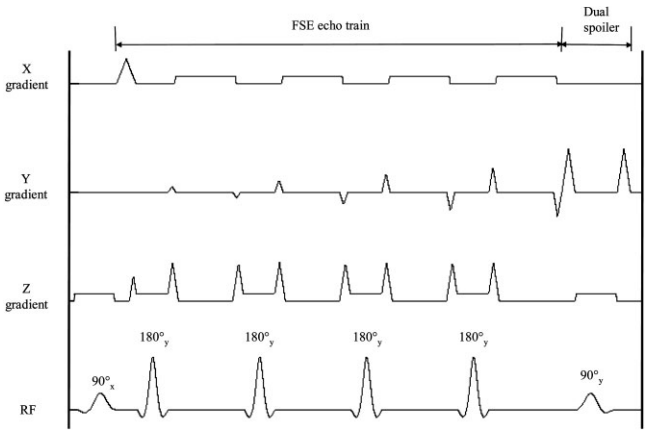

FIG. 2. The TESO-IRFSE T_1 mapping sequence echo train.

Right before the 90° acquisition RF pulse is applied, the longitudinal magnetization is,

$$M_{\text{acq}} = M_0(1 - e^{-\text{TI}/T_1}) - f_{\text{inv}} \cdot M_{\text{Before\_IR}} \cdot e^{-TI/T_1},$$

where f_{inv} = the effective spin inversion fraction. The f_{inv} is applied separately for different voxels or ROIs to accommodate the slice inversion variations due to system imperfection and tissue dielectric effects (13).

Thus,

$$M_{\text{acq}} = M_0\left[(1 - e^{-\text{TI}/T_1}) - f_{\text{inv}} \cdot (1 - e^{-T_{\text{SP\_to\_Before\_IR}}/T_1}) \cdot e^{-\text{TI}/T_1}\right]. \quad [1]$$

Then the voxel or ROI signal measured at the time of echo (TE) is

$$S = k \cdot M_{\text{acq}} \cdot e^{-\text{TE}/T_2},$$

where k = a scaling constant that is dependent on the hardware, scan setting, and image reconstruction.

Thus,

$$S = k \cdot M_0 \cdot e^{-\text{TE}/T_2} \cdot \left[(1 - e^{-\text{TI}/T_1}) - f_{\text{inv}} \cdot (1 - e^{-T_{\text{SP\_to\_Before\_IR}}/T_1}) \cdot e^{-\text{TI}/T_1}\right].$$

The dependency on k, M_0, TE, and T_2 is removed by the normalization process based on the ratio of

$$R_{\text{i\_longest}} = \frac{S(i)}{S(\text{longest})} = \frac{(1 - e^{-\text{TI}(i)/T_1}) - f_{\text{inv}} \cdot (1 - e^{-T_{\text{SP\_to\_Before\_IR}}(i)/T_1}) \cdot e^{-\text{TI}(i)/T_1}}{(1 - e^{-\text{TI(longest)}/T_1}) - f_{\text{inv}} \cdot (1 - e^{-T_{\text{SP\_to\_Before\_IR}}(\text{longest})/T_1}) \cdot e^{-\text{TI(longest)}/T_1}}, \quad [2]$$

where i and "longest" are indices referring to the ith and the longest TI conditions, respectively, with $i = 1, 2, 3, \ldots,$ longest.

Magnitude images are used for T_1 map generation. The curve fitting is based on the comparison between the expected and measured absolute signal ratio,

Table 1
Phantom T_1 Comparison Study between IRSE and TESO-IRFSE at 3T

Scan time/phantom	T_2 (ms)	T_1 (ms) from IRSE	T_1 (ms) from TESO-IRFSE with 3s TR 2 ETL	T_1 (ms) from TESO-IRFSE with 3s TR 4 ETL	T_1 (ms) from TESO-IRFSE with 4s TR 8 ETL
Scan time		1 slice 6 × (5 min 50 s)	12 slices 20 min 15 s	12 slices 10 min 27 s	12 slices 6 min 32 s
2.0 mM Ni^{2+}, 0.95% agarose*	91.6 ± 0.3	612	607 ± 11 (−0.82%)†	602 ± 12 (−1.72%)	597 ± 7 (−2.53%)
1.5 mM Ni^{2+}, 0.95% agarose	95.8 ± 0.6	756	757 ± 13 (0.13%)	751 ± 9 (−0.66%)	749 ± 4 (−0.93%)
1.0 mM Ni^{2+}, 2% agarose	59.1 ± 0.9	976	961 ± 11 (−1.59%)	951 ± 10 (−2.61%)	941 ± 8 (−3.64%)
1.0 mM Ni^{2+}, 1.5% agarose	74.6 ± 0.5	964	960 ± 22 (−0.47%)	947 ± 15 (−1.76%)	932 ± 11 (−3.32%)
0.5 mM Ni^{2+}, 1.5% agarose	78.4 ± 1.0	1412	1390 ± 38 (−1.56%)	1359 ± 21 (−3.75%)	1338 ± 20 (−5.24%)
0.5 mM Ni^{2+}, 0.95% agarose	105.6 ± 0.6	1460	1450 ± 32 (−0.72%)	1433 ± 29 (−1.85%)	1422 ± 12 (−2.60%)

*Agarose is in weight/volume %.
†The T_1 % difference compared to IRSE is indicated inside parentheses after each T_1 value.

$R_{i\_\mathrm{longest,theory}}$ and $R_{i\_\mathrm{longest,measure}}$, respectively, at a voxel or ROI. The T_1 and f_{inv} are obtained when the minimum $\sum_{i=1}^{\mathrm{longest}-1} \| R_{i\_\mathrm{longest,measure}} \| - \| R_{i\_\mathrm{longest,theory}} \|$ is reached.

Phantom and Human Subject Evaluation Studies

The TESO-IRFSE pulse sequence has been implemented on GE Signa 3- and 1.5-T MR imagers equipped with standard quadrature birdcage head coils (GE Medical Systems, Milwaukee, WI, USA). A phantom verification study with three different choices of ETL (2, 4, and 8) was first done on a 3-T system and compared against the traditional single-slice IRSE T_1 mapping technique (also with nonselective spin inversion), which is often utilized as a standard when a new T_1 mapping technique is developed (7,9). The phantoms were prepared in 250-mL plastic bottles with various concentrations of agarose and nickel chloride ($NiCl_2$) to achieve various T_1 and T_2 characteristics. Potassium sorbate (0.1 wt/vol %) was added to each bottle as a preservative. All images were collected with a matrix size of 256 × 128, a 4-mm slice thickness with 4-mm gaps, and a 28-cm field of view (FOV). The IRSE protocol had TE = 15 ms, TR = 2.5 s, receiver bandwidth = ±15.63 kHz, and TI = 100, 400, 700, 1000, 1300, and 1600 ms. The TESO-IRFSE protocols had 12 slices, TE = 8.1 ms, receiver bandwidth = ±31.25 kHz, and 50 ms between the spin inversion and the start of the multislice FSE echo train (equal to TI_1 in Fig. 1); for ETL = 2 or 4, TR = 3 s; for ETL = 8, TR = 4 s. The T_2 values were also evaluated through a semi-log linear regression technique based on the multislice SE images collected at four different TE choices (20, 70, 120, and 170 ms) at the same slice locations with the same slice thickness, slice gaps, and matrix size; the other parameters were TR = 3 s and receiver bandwidth = ±15.63 kHz. Additionally, the effect of slice gap size on T_1 estimation was also evaluated with the slice gap increased to 8 mm from 4 mm for the 4-ETL protocol.

For IRSE T_1 mapping, the same image signal normalization process as for IRFSE was applied to remove the dependency on k, M_0, TE, and T_2. The expected theoretical signal ratio was calculated faithfully according to the longitudinal magnetization evolution, also taking into consideration the effect of the 180° refocusing RF pulse on the longitudinal magnetization. Then T_1 and f_{inv} were obtained based on the same curve fitting procedure as described for IRFSE.

Twelve normal subject studies (7 males, 5 females, and 34.3 ± 9.4 years old) were done with the 4-ETL TESO-IRFSE and 24-cm FOV (other parameters were the same as the phantom study) on the 3-T system. Five normal subjects (3 males, 2 females, 43.4 ± 9.0 years old) were scanned on the 1.5-T system with the same protocol to verify the applicability of the TESO-IRFSE technique to lower field strengths. All volunteers signed the consent forms of research agreement that had been approved by the Institutional Review Board at the University of Chicago. On the 3-T system, 3 of these subjects were imaged first with the 4-ETL protocol and then were imaged again with the 2-ETL and 8-ETL protocols at the same slice locations. The potential underestimation or overestimation of the T_1 value was evaluated when a long ETL protocol was used. After about 40 min, images were acquired again with the 4-ETL protocol to evaluate the reproducibility. The effects of slice gap and ESP on T_1 estimation were further evaluated on the 1.5-T system with 3 subjects and on the 3T system with 5 subjects. As with the phantom study, this comparison utilized the 4-ETL protocol. Images were collected with the slice gap increased to 8 mm. With the 4-mm gap size, images were then collected with the ESP and TE increased to 15 ms.

RESULTS

Table 1 shows the phantom T_1 comparison study between IRSE and TESO-IRFSE at 3 T. With the TESO-IRFSE technique, the scan time efficiency is much improved, for example, from a total of 35 min for one slice when the IRSE protocol was used to 10.45 min for 12 slices (or 0.87 min per slice) when the TESO-IRFSE 4-ETL protocol was used. The phantoms were prepared with a T_2 range from approximately 59 to 106 ms and a T_1 range of approximately 610 to 1460 ms, which are within the ranges for brain tissue (14). For all TESO-IRFSE protocols, the T_1 measurements from the 2-ETL protocol were closest to those from the IRSE, with a maximum variation of only 1.59% (at the T_2 of 59.1 ms) and a mean variation of only 0.88%. The T_1 measurements from the 2-ETL protocol can thus reasonably be considered the true T_1. For the 4-ETL and 8-ETL protocols, the maximum variations are 3.75 and 5.24% (at the T_2 of 78.4 ms), and the mean variations are 2.06 and 3.04%, respectively. T_1 underestimation appears to increase with ETL. The T_1 underestimation is even higher for brain tissue, especially at 3 T (Table 2). Correction for the T_1 underestimation can be made based on the experimental data from human brains.

Table 2
Normal Head Studies with the 4-ETL TESO-IRFSE Protocol and Comparison with Literature

	Frontal white matter	Posterior white matter	Genu of corpus callosum	Splenium of corpus callosum	Head of caudate nucleus	Putamen	Thalamus	White matter of brain overall	Gray matter of brain overall
T_1 (ms) at 3T before correction*	710 ± 23	737 ± 20	675 ± 30	695 ± 22	1110 ± 38	1053 ± 39	965 ± 34	737 ± 20	1325 ± 40
Corrected T_1 (ms) at 3T†	761 ± 25	791 ± 22	724 ± 33	746 ± 24	1190 ± 41	1129 ± 42	1034 ± 37	790 ± 21	1421 ± 43
T_1 (ms) at 1.5T**	568 ± 27	592 ± 21	543 ± 25	565 ± 17	924 ± 28	854 ± 13	782 ± 19	593 ± 17	1106 ± 52
T_1 (ms) at 3T from Wansapura et al. (14)								832 ± 10	1331 ± 13
T_1 (ms) at 1.5T from the "gold standard" technique in Steen et al. (6)		606 ± 21	546 ± 28		948 ± 32	834 ± 19	774 ± 16		1170 ± 43
T_1 (ms) at 1.5T from the PAIR technique in Steen et al. (6)	555 ± 17	588 ± 19	544 ± 24	565 ± 21	928 ± 26	817 ± 51	758 ± 24		1013 ± 62

*Based on 12 subjects.
†T_1 after applying the correction equation (Eq. (3)).
**Based on five subjects.

Using 9 ROIs (see Table 2) on three subjects (a total of 27 ROIs), the 4-ETL and 8-ETL T_1 measurements differ from the 2-ETL measurements by 6.71 ± 1.39 and 11.7 ± 2.3%, respectively. A clear linear relationship between the longitudinal relaxation rate R_1 (=1/T_1) obtained from the 4-ETL or 8-ETL protocol and that from the 2-ETL protocol was also found based on these ROIs (Fig. 3). To reduce the T_1 underestimation, the R_1 measured from other two protocols can be converted to the equivalent measurement with the 2-ETL protocol through these linear relationships based on the results of linear regression,

$$R_{1\_2ETL} = 6.57 \times 10^{-4} + 0.932 \times R_{1\_4ETL}, \quad [3]$$

with a standard error of estimate of 1.33%, and

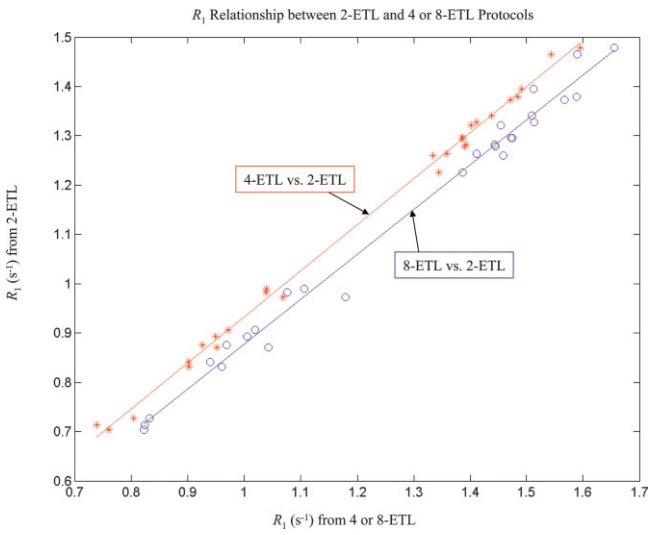

FIG. 3. The R_1 linear relationship between 2-ETL and 4-ETL or 8-ETL protocols.

$$R_{1\_2ETL} = -0.0314 + 0.909 \times R_{1\_8ETL}, \quad [4]$$

with a standard error of estimate of 2.48%, where R_{1_2ETL} = the corrected R_1 measurement equivalent to the 2-ETL protocol, R_{1_4ETL} = the R_1 measurement directly from the 4-ETL protocol before correction, and R_{1_8ETL} = the R_1 measurement directly from the 8-ETL protocol before correction. The low standard error of estimate of 1.33% suggests that the conversion of T_1 from the 4-ETL to 2-ETL protocol is highly reliable. The 2.48% standard error of estimate suggests that Eq. [4] is still reasonably reliable for the T_1 conversion from the 8-ETL to the 2-ETL protocol.

Besides a long ETL, narrow slice gap size can cause the underestimation of T_1. For the 4-ETL protocol, reducing the slice gap size from 8 to 4 mm leads to a T_1 reduction of 2.33 ± 0.27% in white matter and 3.40 ± 2.50% in gray matter at 1.5 T (based on three normal subjects), a T_1 reduction of 4.53 ± 0.45% in white matter and 5.24 ± 1.55% in gray matter at 3 T (based on five normal subjects), and only 0.901 ± 0.468% for the gel phantoms at 3 T. The ESP contribution to the T_1 underestimation was negligible. Less than 1% reduction in gray and white matter overall was measured due to the increase of ESP from 8.1 to 15 ms at both field strengths.

The TESO-IRFSE technique is highly sensitive to tissue T_1 difference. For example, a T_1 difference between the frontal and posterior white matter was found, as previously observed by other groups (3,6). The technique has also shown be highly reproducible. The retest with the 4-ETL protocol shows a variation (the absolute difference) of 0.909 ± 0.626% from the 7 ROIs (as in Table 2) of the three subjects (a total of 21 ROIs).

The effective spin inversion fraction f_{inv} in Eq. [1] was found to vary among tissue types and field strengths, based on data from three subjects at 1.5 T and another three subjects at 3 T, both with the 4-ETL 8-mm gap protocol.

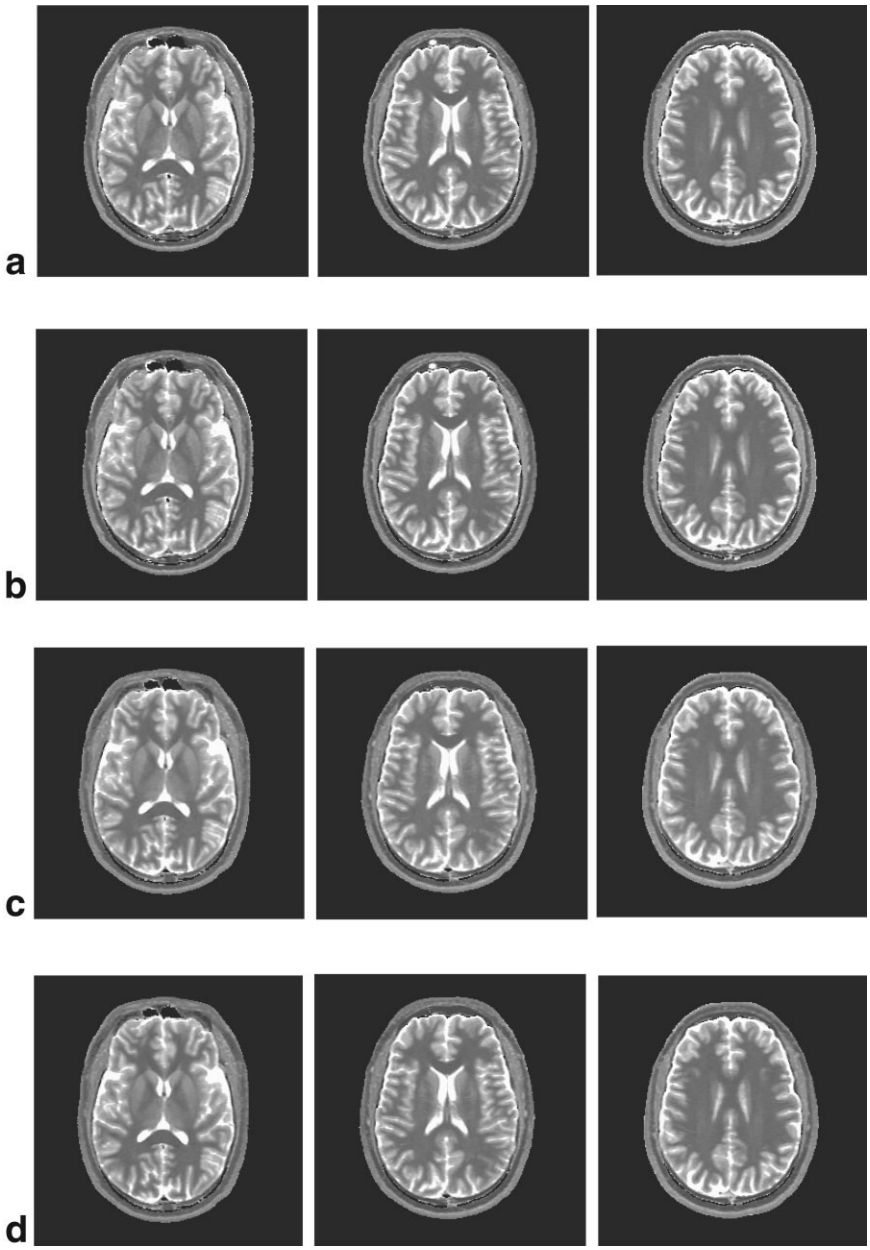

FIG. 4. Three of the 12 T_1 maps obtained with the TESO-IRFSE technique at 3 T: (**a**) T_1 maps generated directly from images obtained with the 4-ETL protocol, (**b**) after the application of the T_1 correction equation (Eq. [3]) to (a), (**c**) T_1 maps generated directly from images obtained with the 8-ETL protocol, and (**d**) after the application of the T_1 correction equation (Eq. [4]) to (c).

For each subject study, the transmit gain was optimized to achieve "perfect" inversion. At 1.5 T, the f_{inv} values were found to be 90.9 ± 1.1% for white matter, 93.6 ± 0.3% for gray matter, and 98.2 ± 0.6% for cerebrospinal fluid. At 3 T, the corresponding values were 86.9 ± 0.6, 91.4 ± 0.4, and 98.0 ± 0.6%.

High-quality T_1 maps from the 4-ETL and 8-ETL protocols have been generated (Fig. 4). The corrected T_1 maps from 4-ETL and 8-ETL protocols based on Eqs. [3] and [4] also demonstrate the applicability of the conversion to achieve more accurate T_1 maps. These T_1 maps qualitatively show the same tissue contrast across all four cases at the same slice locations.

DISCUSSION

The results demonstrate that the proposed TESO-IRFSE technique is capable of providing precise and highly reproducible T_1 maps with an efficient usage of scan time. A standard IRSE technique takes 35 min to collect the necessary data for one slice. With TESO-IRFSE, the 8-ETL protocol requires only 6 min 32 s to study 12 slices, and the 4-ETL protocol requires only 10 min 27 s to study 12 slices. In both protocols, we scanned 12 4-mm-thick slices with gaps of 4 mm. To study the full brain with no gaps, a second set of 12 slices is collected to fill the gaps. The resulting total scan time is 13 min 4 s for the 8-ETL protocol and 20 min 54 s for the 4-ETL protocol. This is less than 1/40 of the scan time necessary using the standard IRSE technique that provides a similar T_1 map SNR. This scan time efficiency has been achieved by taking advantage of the difference in slice acquisition time. Although the slice acquisition always starts with the same short delay after the nonselective RF inversion, the slices are affected by different TIs. By sorting the order of the slice acquisition properly, various TI values can be obtained for

T_1 mapping. To further improve the scan time efficiency for full-brain coverage, a longer ETL, more slices, and a reduced number of TI choices can also be used, but the accuracy and precision of the protocol should be evaluated and the values might need to be corrected. The minimum scan time is ultimately limited by the fact that FSE requires RF refocusing pulses, compared to the full-brain EPI based technique by Clare and Jezzard (1). If only a few slices are imaged, the scan time efficiency of the TESO-IRFSE technique might be reduced. This is because the technique requires the total number of slices to be equal to the multiplication of the number of TI steps by the number of slices in each TI increment.

The TESO-IRFSE technique has been designed to take advantage of high-quality spin echo images that are much less prone to magnetic field inhomogeneity than the gradient-echo images that are used in the Look and Locker or other approaches. This feature obviously becomes advantageous when magnetic field homogeneity is an issue. The TESO-IRFSE technique uses 90° excitation RF pulses, which maximize the image SNR, compared to excitation RF pulses with low flip angles that are used in the Look and Locker approach (7).

Brain T_1 values are systematically underestimated in the proposed TESO-IRFSE technique in both 1.5- and 3-T fields. The T_1 measurements by Steen at al (6). at 1.5 T and by Wansapura at el. at 3 T (14) were accompanied by vigorous verification steps and thus are included in Table 2 for comparison. The T_1 brain values measured by us at 1.5 T (Table 2) show good agreement with the results of Steen et al. (6), although they are slightly less than Steen's results using the "gold standard" technique (an IRSE method with a 6-s TR and 12 TI steps). Both our measurements and those by Steen et al. are significantly lower than those of Breger et al. (15) with the white matter T_1 values in the range of 742–764 ms and also lower than those of Vymazal et al. (16) with a white matter T_1 value of 660 ± 51 ms. The T_1 values (before correction) at 3 T with the 4-ETL protocol were obviously systematically lower than those measured by other groups (1,14); a much closer correspondence was obtained after applying the correction equation (Eq. [3]). Although a longer ESP can contribute to the T_1 mapping imprecision due to image blurring, it was not found to contribute to the T_1 underestimation. This underestimation is due to the assumption that spins at the acquisition slice are not influenced by spins outside the slice. One important factor is the interslice interference. Specifically, the excitation and the refocusing RF pulses do not have perfect slice profiles. Thus, the slices that are acquired at the later part of the TR period can be excited by small flip angles due to neighbor slices that were acquired earlier. If these spins are still at the negative half of the recovery curve, they would recover faster. To reduce the interslice interference, two approaches can be applied. One is to reduce the ETL so that the frequency of small-flip-angle excitation is reduced. Using the protocol with a slice gap of 4 mm, the T_1 values at 4 ETL is 6.71 ± 1.39% less than those at 2 ETL in the brain. The other approach is to choose a reasonable slice gap size. With the 4-ETL protocol, reducing the gap size from 8 to 4 mm led to a T_1 reduction of 4.53 ± 0.45% in white matter and 5.24 ± 1.55% in gray matter at 3 T. However, the slice gap size has a less effect with the gel phantom. The T_1 value was reduced by only 0.901 ± 0.468% after the slice gap was reduced from 8 to 4 mm. This difference is probably due to perfusion, which is not present in the gel phantoms. In the brain, due to the effect of perfusion, the spins at the acquisition slice constantly exchange with spins outside the slice that are in different states of longitudinal magnetization. For a simple case with proximal saturation and with the effect of magnetization transfer ignored, the apparent or measured T_1 (T_{1app}) and the true T_1 at an acquisition slice have the relationship of

$$\frac{1}{T_1} = \frac{1}{T_{1app}} - \frac{f}{\lambda},$$

where f/λ = the perfusion effect (17). However, this simple relationship cannot be applied directly to the more complicated situation when the TESO-IRFSE sequence is applied. The states of spin longitudinal magnetization are different at the acquisition slice, the slice gap, and the neighbor slices and also vary with the number of refocusing pulses applied (the ETL). Although the degree to which each factor contributes to the underestimation of the T_1 cannot be quantified by a simple correction algorithm, the total underestimation is small. The simple T_1 relationship to perfusion above can be expanded to model the relationship between the true T_1 and T_{1app} through a first degree of approximation,

$$\frac{1}{T_1} = \frac{A}{T_{1app}} + B,$$

where the "true" T_1 can be obtained from a protocol with a low T_1 underestimation, such as the one with a short ETL and/or large slice gaps. The A and B are constants to be found through linear regression. In our study, we treated the T_1 obtained with the 2-ETL protocol as the true T_1. The resulting linear relationship was used to correct our measurements with protocols having higher numbers of ETL. The same anatomic regions were compared. Although a complete correction cannot be assumed, the degree of underestimation has been reduced significantly. The low standard errors of estimate of these conversions (Eqs. [3] and [4]) also validate this approach. An alternative approach for the conversion is to apply the linear regression directly between T_1 and T_{1app}. The standard errors of estimate in fact were still low, but are not as good as the other approach (1.84% versus 1.33% for the 4- to 2-ETL linear regression and 2.64% versus 2.48% for the 8- to 2-ETL linear regression).

The effective spin inversion fraction f_{inv} in Eq. [1] was found to vary due to tissue types and field strengths, and it is certainly less than 100% if the RF transmitting gain was not optimized to deliver a "perfect" flip angle during the scan tuning step. To calculate T_1 accurately by curve fitting, therefore, it was important to include f_{inv}, even though an adiabatic inversion pulse was used. Our finding agrees with those of Clare and Jezzard. (1). In choosing the TR, a sufficient signal recovery time after the spin inversion should be considered, and the range of TI choices resulting from the choice of TR should reasonably map the

longitudinal magnetization recovery curve appropriate for the brain tissue T_1. The 3-T system offers an improved SNR and thus can improve the precision of T_1 mapping over the 1.5-T system. However, the TESO-IRFSE technique proposed here applies RF pulses frequently and thus scan time efficiency may be limited in some cases by the higher RF power deposition at 3 T.

Our TESO-IRFSE technique has successfully increased the scan time efficiency compared to the conventional IRSE and IRFSE T_1 mapping techniques, and it produces precise and highly reproducible full-brain T_1 maps. The accuracy can be improved using linear correction methods. We are now applying this technique to brain water content measurements under pathologic conditions.

ACKNOWLEDGMENTS

We thank Dr. Anthony Vu for helpful discussion on IR pulses, Dr. Steven Tan for helpful discussion on FSE sequences, Dr. David Wright for help in making the gel phantoms, Dr. Timothy Skloss for the suggestions on gel phantom materials, and Mr. Robert Lyons for scanning support.

REFERENCES

1. Clare S, Jezzard P. Rapid T_1 mapping using multislice echo planar imaging. Magn Reson Med 2001;45:630–634.
2. Constable RT, Smith RC, Gore JC. Signal-to-noise and contrast in fast spin echo (FSE) and inversion recovery FSE imaging. J Comput Assist Tomogr 1992;16:41–47.
3. Fatouros PP, Marmarou A. Use of magnetic resonance imaging for in vivo measurements of water content in human brain: method and normal values. J Neurosurg 1999;90:109–115.
4. Schwarcz A, Berente Z, Osz E, Doczi T. Fast in vivo water quantification in rat brain oedema based on T_1 measurement at high magnetic field. Acta Neurochir 2002;144:811–816.
5. Steen RG, Hunte M, Traipe E, Hurh P, Wu S, Bilaniuk L, Haselgrove J. Brain T_1 in young children with sickle cell disease: evidence of early abnormalities in brain development. Magn Reson Imaging 2004;22: 299–306.
6. Steen RG, Gronemeyer SA, Kingsley PB, Reddick WE, Langston JS, Taylor JS. Precise and accurate measurement of proton T1 in human brain in vivo: validation and preliminary clinical application. J Magn Reson Imaging 1994;4:681–691.
7. Henderson E, McKinnon G, Lee TY, Rutt BK. A fast 3D Look-Locker method for volumetric T_1 mapping. Magn Reson Imaging 1999;17: 1163–1171.
8. Zhu DC, Buonocore MH. Breast tissue differentiation using arterial spin tagging. Magn Reson Med 2003;50:966–975.
9. Deoni SC, Rutt BK, Peters TM. Rapid combined T_1 and T_2 mapping using gradient recalled acquisition in the steady state. Magn Reson Med 2003;49:515–526.
10. Silver MS, Joseph RI, Hoult DI. Highly selective $\pi/2$ and π pulse generation. J Magn Reson 1984;59:347–351.
11. Listerud J, Einstein S, Outwater E, Kressel HY. First principles of fast spin echo. Magn Reson Q 1992;8:199–244. Review.
12. Zhou XJ, Tan SG, Bernstein MA. Artifacts induced by concomitant magnetic field in fast spin-echo imaging. Magn Reson Med 1998;40: 582–591.
13. Roschmann P. Radiofrequency penetration and absorption in the human body: limitations to high-field whole-body nuclear magnetic resonance imaging. Med Phys 1987;14:922–931.
14. Wansapura JP, Holland SK, Dunn RS, Ball WS Jr. NMR relaxation times in the human brain at 3.0 Tesla. J Magn Reson Imaging 1999; 9:531–538.
15. Breger RK, Yetkin FZ, Fischer ME, Papke RA, Haughton VM, Rimm AA. T1 and T2 in the cerebrum: correlation with age, gender, and demographic factors. Radiology 1991;181:545–547.
16. Vymazal J, Righini A, Brooks RA, Canesi M, Mariani C, Leonardi M, Pezzoli G. T1 and T2 in the brain of healthy subjects, patients with Parkinson disease, and patients with multiple system atrophy: relation to iron content. Radiology 1999;211:489–495.
17. Detre JA, Leigh LS, Williams DS, Koretsky AP. Perfusion imaging. Magn Reson Med 1992;23:37–45.